Published in final edited form as:
Biomaterials. 2011 January ; 32(3): 681–692. doi:10.1016/j.biomaterials.2010.09.033.

The Surface Immobilization of the Neural Adhesion Molecule L1 on Neural Probes and its Effect on Neuronal Density and Gliosis at the Probe/Tissue Interface

Erdrin Azemi[a,c,*], **Carl Lagenaur**[b,c], and **Xinyan Tracy Cui**[a,c,d]

[a] Department of Bioengineering, University of Pittsburgh, Pittsburgh, PA 15261, USA

[b] Department of Neurobiology, University of Pittsburgh, Pittsburgh, PA 15213, USA

[c] Center for the Neural Basis of Cognition, Pittsburgh, PA 15261, USA

[d] McGowan Institute for Regenerative Medicine, Pittsburgh, PA 15203, USA

Abstract

Brain tissue inflammatory responses, including neuronal loss and gliosis at the neural electrode/tissue interface, limit the recording stability and longevity of neural probes. The neural adhesion molecule L1 specifically promotes neurite outgrowth and neuronal survival. In this study, we covalently immobilized L1 on the surface of silicon based neural probes and compared the tissue response between L1 modified and non-modified probes implanted in the rat cortex after 1, 4, and 8 weeks. The effect of L1 on neuronal health and survival, and glial cell reactions were evaluated with immunohistochemistry and quantitative image analysis. Similar to previous findings, persistent glial activation and significant decreases of neuronal and axonal densities were found at the vicinity of the non-modified probes. In contrast, the immediate area (100 μm) around the L1 modified probe showed no loss of neuronal bodies and a significantly increased axonal density relative to background. In this same region, immunohistochemistry analyses show a significantly lower activation of microglia and reaction of astrocytes around the L1 modified probes when compared to the control probes. These improvements in tissue reaction induced by the L1 coating are likely to lead to improved functionality of the implanted neural electrodes during chronic recordings.

Keywords

L1; glial encapsulation; neurodegeneration; axon regeneration; neural probes

1. Introduction

Neural interface technologies are being developed to record neural signals from the brain and decode these signals into controlled movements of a computer cursor, a robot, or an artificial limb [1]. These technologies are currently at the early stage of human clinical trials [2-7] and are designed as assistive means intended to help patients suffering from spinal

[*]Corresponding author. Tel.: +1 412 527 0104; fax: +1 412 383 5918. erdrin.azemi@gmail.com.

cord injury, degenerative disorders, strokes interrupting descending motor pathways, and/or limb amputation(s) [4-12].

Chronic recordings via microfabricated neural probes are known to deteriorate over time, regardless of electrode or the animal model employed [13-16]. The lifetime of electrode recordings has been reported to last from a few weeks up to several months [1, 17]. A potential explanation for recording failure is thought to be the loss of neurons surrounding the electrodes over time [13-15]. As neural recordings require proximity between the electrode and the neuron (<100 μm), loss of neurons near the implant leads to the loss of reliable signals [13]. Another possible cause of reduced electrode performance is chronic gliosis, which results in a dense cellular sheath that encapsulates the neural probe and isolates it from the surrounding brain tissue [13-15, 18]. Gliosis is mediated by macrophages, activated microglia, and reactive astrocytes [14, 17]. Activated microglia and macrophages are found to be concentrated at the electrode-tissue interface throughout the implantation period. In addition, reactive astrocytes form a tight sheath around the implant, which tends to stabilize after a few weeks. Although the activation of glial cells in response to brain injury occurs to prevent further tissue damage, they are known to release pro-inflammatory and neurotoxic factors that lead to neuronal death and degeneration as well as factors that may inhibit axonal re-growth and regeneration [19-21].

Strategies to alter the implant surface are being developed to achieve chronically stable electrode-tissue interfaces. Approaches to reduce the glial reaction include coating the electrodes with bioactive molecules or anti-inflammatory compounds [14]. For example, conductive polymers doped with peptides grown on the surface of electrode sites on silicon-substrate microelectrodes have shown to improve the electrode-neuron connection [22-24]. The extra cellular matrix protein, laminin, was deposited on the surface of the neural probes using a layer-by-layer deposition technique [25]. Laminin alleviated the prevalence of gliosis but did not improve neuronal density around the implantation site at chronic time points. A potent anti-inflammatory peptide alpha-melanocyte stimulating hormone (MSH) was coated on the surface of neural electrodes [26]. MSH coating demonstrated the capacity to reduce ED-1 staining of activated microglia and GFAP staining of astrocytes *in vivo*. Also, anti-inflammatory drugs such as dexamethasone have been used locally and systemically to reduce activation of astrocytes and microglia at the implantation site [27-31]. The long-term effect of this anti-inflammatory drug on neurons and neural recording remains to be determined. Purcell *et al.* reported the novel use of the drug Flavopiridol, a cell cycle inhibitor, which showed some improvement of glial activation but with no improvement on neural recordings [32]. Although the above-mentioned methods have shown promise in the field, it is still considered a challenge to achieve long-term reliable connections between the probe and the brain tissue at the cellular and/or biomolecular level.

In this study, we propose a novel method to improve the implant-tissue interface by introducing the neural cell adhesion molecule L1 onto the probe's surface. L1 is expressed in most neurons in the central nervous system (CNS), and targeted on the surface of developing axons and growth cones during development. L1 is known to mediate axon outgrowth, adhesion, fasciculation, including axonal guidance and neuronal migration and survival [33-36]. L1 has also been suggested to promote CNS regeneration in adult vertebrates. During a study using zebrafish models with spinal cord injuries, the expression of a homolog of the mammalian L1 was observed to increase in the successfully regenerating descending axons but not in the ascending non-regenerating projections [37]. Enhanced recovery of rats from spinal cord injury were achieved when: 1) L1 expression in neurons and glia was induced by viral transduction [38], 2) L1 overexpressing embryonic stem cells were transplanted [39], and 3) the axonal growth-inhibiting environment was

enriched with exogenous L1 [40]. These findings indicate that L1 is a molecule that promotes CNS regeneration and/or prevents neuronal death.

During previous *in vitro* work, we have reported that the immobilized L1 molecule on silicon substrates supports primary neuronal growth and promotes neurite extension, while suppressing glial cell attachment [41]. We hypothesize that L1 immobilized on the surface of neural probes will promote neuronal growth on and around the electrode, and induce axonal regeneration after implantation induced injury. Maintaining neuronal density and neuronal health around the implant may reduce adhesion and activation of glial cells. The presence of L1 may also directly inhibit glial cell attachment and reduce gliosis. To test these hypotheses, L1 modified neural probes and non-modified (NM) control probes were implanted in rat cortex for 1, 4, and 8 weeks. The cellular tissue response was evaluated for the L1 probes and compared to NM controls after each time point.

2. Materials and Methods

2.1. Neural probes and L1 modification

Experimental studies were performed using NeuroNexus chronic supplementary kits (NeuroNexus Technologies, Ann Arbor, MI) consisting of four-shank silicon-based neural probes mounted on dummy boards. The dummy boards were similar in size and shape to the actual percutaneous connectors except lacking electrical connections. The design and fabrication of these probes have been previously described in Drake *et al.* [42]. Probe dimensions consisted of implant thickness of 15 μm, shank length of 4mm, and tip spacing of 200 μm.

Prior to all procedures the probes were sterilized via ethylene oxide (EtO*)* sterilization. L1 immobilization was performed on the silicon dioxide surface of the probes using silane chemistry and the hetero-bifunctional cross-linking reagent, 4-maleimidobutyric acid N-hydroxysuccinimide ester (GMBS) (Sigma Aldrich, USA) as previously reported [41, 43]. Briefly, after cleaning and hydroxylation of the silicon dioxide surface with HNO_3 (Sigma Aldrich), the probes were carefully immersed in a 2% solution of (3-mercaptopropyl) trimethoxysilane (MTS) (Sigma Aldrich) and treated for 1 hour with 2 mM of GMBS. L1 (100 μg/ml) (purified at our laboratory) was applied for 1 hour at 4°C on the GMBS treated surface. The L1 imm obilized probes were rinsed with PBS (pH 7.4), and treated with 100 μM Poly(ethylene glycol)-NH_2 (PEG-NH_2) (JenKem, Allen, TX) solution for 30 min to cap any active NHS ester groups of the GMBS. The L1 modified probes were implanted immediately after this process.

2.2. Surgical procedures

Twelve adult male Sprague-Dawley rats (250 ± 20 g) were used throughout this study. Four animals per time point were implanted on each hemisphere with either a NM probe or L1 modified probe. Three end points were investigated: 1 week, 4 weeks, and 8 weeks. These endpoints were chosen to observe the acute (1 week) and chronic tissue responses (4 and 8 weeks). The animals were housed in the facilities of the University of Pittsburgh Department of Laboratory Animal Resources and given free access to food and water. All experimental procedures complied with the United States Department of Agriculture guidelines and were approved by the University of Pittsburgh's Institutional Animal Care and Use Committee. The probe implantation techniques were followed as previously described in Vetter *et al.* [16]. The NM or L1 modified probes were implanted in the motor area of the cerebral cortex of the animal. General anesthesia was achieved with a mixture of 5% isoflurane in 1 L min^{-1} O_2 for 5 minutes prior to implantation surgery and maintained to effect (1-3% isoflurane). The state of anesthesia was closely monitored throughout the procedure

observing the animals for changes in respiratory rate, heart rate, and absence of the pedal reflex. The animals were placed into a stereotaxic frame and their head was shaved over the incision area. The skin was disinfected with isopropyl alcohol and betadine and a sterile environment was maintained throughout the procedure. Ophthalmic ointment was applied to the eyes. An incision was made along the scalp and the skin was retracted to expose the bregma and midline. A 2 mm × 2 mm craniotomy was hand-drilled above the motor cortex (coordinates from bregma: AP: −0.5, ML: ± 2.5-3.5). This method provided for a more controlled craniotomy than the iatrogenic damage caused while using electric drills. For each rat, one L1 probe was implanted on one cortical hemisphere while a NM probe was implanted on the contralateral side. Several stainless steel bone screws were placed in the skull to retain the dental acrylic head-cap and mimic functional probe surgical tethering procedures. The dura layer was incised using a fine dura pick (Fine Science Tools, USA). The probe was inserted manually into the motor cortex using Teflon-coated micro-forceps. To minimize bleeding and severe tissue reaction, blood vessels visible on the cortical surface were avoided during probe insertion. The craniotomy was filled with the noncytotoxic silicone elastomer, Kwik-Sil (World Precision Instruments, Sarasota, FL), followed by dental acrylic (Henry Schein, Melville, NY) (Figure 1). The overlying skin was sutured around the dental acrylic head-cap and the animal was allowed to recover under close observation in the surgical procedure room. To minimize variability associated with the surgery, all implantations were performed by the same surgeon.

2.3. Immunohistochemistry

After each time point (1/4/8 weeks), animals were anesthetized with 50 mg/ml ketamine, 5 mg/ml xylazine, and 1 mg/ml acepromazine (Henry Schein) administered via the intraperitoneal (IP) cavity with the dosage of 0.1 ml/100 g body weight. The animals were transcardially perfused with 4°C PBS p rewash followed by 4% (w/v) paraformaldehyde in PBS. The brain tissue was removed and postfixed overnight (4°C). Following electrode retrieval, brain tissue was equilibrated in 30% sucrose solution (4°C) until it sunk to the bottom and later cryopro tected using the optimal cutting temperature (OCT) compound (Tissue-Tek, Torrance, CA). Serial horizontal sections were cut at a 20 μm thickness to approximately 3 mm cortical depth.

To minimize variability, tissue sections were stained at the same time for each antibody of interest. Six consecutive serial sections were stained for six different cellular markers at four different cortical depths. The markers chosen to visualize the presence of neuronal nuclei (NeuN), astrocytes (GFAP), activated microglia/macrophages (ED-1), mature axons (NF-200), microglia (Iba1), and astrocytes/fibroblasts/endothelial cells (Vimentin) are shown in Table 1.

Tissue sections were hydrated in buffer (PBS), blocked with 10% normal goat serum in PBS for 45 min followed with PBS containing 0.5% Triton X-100 (Sigma). The sections were then incubated overnight with the primary antibodies prepared in blocking solution (4°C) with concentrations shown in Table 1. The next day, sections were rinsed in PBS and incubated for 1 hour in either goat anti-rabbit IgG (H + L) Alexa 488 or goat anti-mouse IgG1 Alexa 488 (Invitrogen, USA) secondary antibodies were diluted at a ratio of 1:200 in blocking solution. All sections were counterstained using Hoechst (Invitrogen) nuclear dye to observe cell nuclei and cover-slipped with Fluoromount-G (Southern Biotechnology Associates, Birmingham, Alabama) to preserve fluorescence over time. Buffer was used in place of primary antibodies for control tissue samples.

Only two L1 probes and 1 NM probe were successfully retrieved after animal perfusion for further qualitative analysis. Difficulty upon retrieval was faced with all probes due to their

delicate material composition. The salvaged probes were stained for β-tubulin III (Table 1) to identify neuronal cells present on the probe's surface.

2.4. Quantitative brain tissue analyses

Confocal fluorescent and optical differential interference contrast (DIC) images were acquired using a Nikon A1 (Nikon Instruments, Inc., Melville, NY) microscope. Images for each specific antibody were taken in a single session to reduce the discrepancy during data analysis. The exposure time of each marker was consistent and was set below the saturation of the digital camera. During laser scanning confocal imaging, each pixel was obtained using the same laser power and detector gain setting for each specific antibody stained tissue. For analysis purposes a 10x objective was used with the electrode sites centered in the camera field. Four sections at different depths in the brain (approximately Depth 1 = 300μm, Depth 2 = 700 m, Depth 3 = 1100μm, and Depth 4 = 1500μm) below the rat cortex surface were imaged per each stain shown in Table 1. This was performed to observe the tissue response at different depths along the shaft of the implanted probes.

Average pixel intensity was calculated as a function of distance from the electrode-tissue interface using the image-processing program, ImageJ (National Institute of Health, Bethesda, MD). A macro was written to perform the desired analysis. Briefly, (GFAP/ED-1/Iba1/NF/Vimentin) stained images were cropped where one out of four probe shank tracks fit within a window of ~1200 μm in height and ~300 μm in width. An outline of the probe-tissue interface was defined by a combination of the DIC and UV fluorescence image (Figure 2A). This outline served as the template at which thereafter 20 μm regions following the same outline shape were segmented up to 520 μm away around the probe-interface. The average gray scale pixel intensity (1-255 a.u.) for all the pixels in the 20 μm areas were calculated and plotted as a function of distance. To correct for background differences and produce unitless values, the average pixel intensity was normalized to a distant uninjured section (420 μm - 520 μm) for each image (also defined as background). All data were averaged across multiple sections from all 4 animals for each time point and depth.

NeuN stained images were quantified by estimating the number of neurons as a function of distance from the electrode interface. NeuN stains for neuronal cell bodies and the NeuN images were processed for cellular counts. Each image was segmented using a marker-based watershed algorithm in ImageJ and the NeuN+ cells were counted at 50 μm increment bins away from the interface up to 600 μm away from each side of the probe's interface (Figure 2B). The results were normalized to the background cellular count (500-600 μm away from the interface) and averaged across results for each time point and depth conditions.

2.5. Statistical analyses

Statistical analyses were performed using the SPSS statistics software (SPSS, Inc., Chicago, IL). For experiments that involved the comparison of two conditions, the standard Student's t-test (α=0.05) was performed. T-test analyses were used to compute p-values comparing NM and L1 data at different distance increments such as 0-100 μm from the interface and up to 400-500 μm away from the implant/tissue interface. Differences were considered significant for $p < 0.05$. T-test analyses were also performed to compare the average data from the 0-100 μm increment distances from the interface with the background data. The background data consisted of the average pixel intensity of the 420 μm - 520 μm distance increments for the NF, GFAP, Vimentin, Iba1 and ED-1 stains. For the NeuN+ cell analyses, background data was considered the average number of NeuN+ cells in the 500-600 μm area from the probe tissue interface.

For comparisons involving multiple conditions, one-way standard analysis of variance (ANOVA) was used. NM or L1 probe data were compared this way through the 3 different time points and also through different depths. When a significant difference was found between groups Tukey's Honest Significant Difference (HSD) post-hoc test was utilized to identify pairwise differences. Differences were considered significant for $p < 0.05$.

3. Results

3.1. Neuron density and axonal immunoreactivity (NeuN and NF)

The impact of electrode implantation on the surrounding neuronal population was assessed by immunostaining for both NeuN, a nuclear antigen found only in neuronal cells, and NF-200, which stains for mature axons. Representative images for NeuN+ cells at the 8-week time point around the L1 and NM probes are shown in figures 3A,B respectively. The normalized cell counts of viable neurons around the implant's interface as a function of distance at different time points are plotted in figures 3D-F. For the NM control probes, neuronal decrease when compared to background tissue were evident within the 200 μm area around the implants at all time points. The L1 modified probes maintained a normal density of neuronal cell bodies around the electrode interface. Significant differences using t-test analysis were found between L1 and NM probes for NeuN+ cell counts at all time points in the area of 0-100 μm around the interface (Table 2). Normalized cell counts within the 100 μm area at all time points for the L1 and NM conditions are plotted in figure 3C. For the NM probe, a lower than background neuronal cell count was observed at all time points, with no statistically significant difference found within time points. For the L1 modified probe, there was an initial slight increase in cell count at week 1 when compared to background (indicated by normalized data in arbitrary units (a.u.)). During the later time points, the neuronal density seemed to reach background levels and remained unchanged.

NF-200 is a marker for mature axons. Representative images for NF staining at the 8-week time point for L1 and NM probes are shown in figures 4A,B. The NF+ axons are increased around the L1 probes interfaces while the NM probes show reduced axonal density. The average gray pixel intensity of NF stain at the 3 different time points was calculated and normalized to the background intensity. L1 modified vs. the NM control probes were plotted as a function of distance (Figures 4D-F). For the NM control implants, we observed reductions in NF reactivity when compared to background levels intensity extending as far away as 200 μm in some cases, but on average this reduction was observed to be significant in the 100 μm area around the implant site. In contrast, for the L1 implants, a mirrored significant increase in the NF staining compared to the background was observed (Figure 4D-F). The p-value differences in NF intensity between the two conditions were compared at different spatial regions away from the electrode-tissue interface (Table 2). In comparison with the L1 probe, mature axons showed a statistically significant lower density around the NM probe within the 100 μm area around the electrode interface at all time points as well as within 100-200 μm area for the first week (Table 2). The integrated NF intensities at the 0-100 μm region around the probes' interfaces for L1 and NM at all 3 time points are illustrated in Figure 4C.

3.2. Astroglia reaction (GFAP and Vimentin)

GFAP, a commonly used marker to visualize astrogliosis, is expressed by mature astrocytes and upregulated after insult. Immature and reactive astrocytes, fibroblasts, microglia, as well as endothelial cells, express the Vimentin marker. This marker in addition to GFAP is generally used to indicate gliosis formation. Representative images of GFAP+ and Vimentin + cells around the L1 and NM probes at the 4-week time point are shown in figures 5A,B and 6A,B, respectively. The average pixel intensities of GFAP and Vimentin stained

sections were quantified as a function of distance from the tissue interface of the probes. Figures 5D-F show the intensity distribution of GFAP+ cells surrounding the insertion site for both L1 and the NM control probes. Figures 6D-F show the intensity distribution of Vimentin+ cells surrounding the probe insertion sites. The average intensity curves are plotted as a function of distance from the implant interface and normalized to the background intensity.

The characteristics of the GFAP expression differed with distance from the electrode at the three different end points (1, 4, and 8 weeks) (Figures 5D-F). After 1 week, the peak of the GFAP intensity curve was found to be as far as 75 μm away from the interface. After 4 weeks, the peak of GFAP expression was closer to the interface (~25 μm). After 8 weeks, the highest expression levels of GFAP were in the immediate vicinity of the probe interface (Figure 5F). This trend was seen around both L1 and NM probes. However, the intensity of the GFAP staining was significantly lower for the L1 coated probes than the NM controls at all time points at the vicinity of the probes (Table 2). This significance was observed only in the 100 μm region around the probe-tissue interface for all time points (Figure 5C).

Vimentin expression showed similar trends as the GFAP reactions for both L1 and NM control probe conditions (Figures 6D-F). One-week post implantation, Vimentin expression for the NM control probe was observed to increase all around the interface, reaching normal intensity values at approximately 150 μm away from the probe's interface. At 4 and 8 weeks, for the NM control probes the normal intensity values were achieved around 100 μm from the interface. The average intensity of Vimentin+ cells was significantly decreased around the L1 modified probes compared to the NM control for all time points within the 100 μm region (Figure 6C).

3.3. Microglia/Macrophage reaction (ED-1 and Iba1)

Microglia form a front line of defense during the acute and chronic inflammatory responses. These cells are known to be part of the persistent glial sheath. ED-1 is a specific marker to detect reactive microglia and/or macrophages. For both L1 and NM probes, most of the ED-1+ cells were observed to be in proximity to the electrode interface site (Figures 7A,B). Comparison of ED-1 immunostaining revealed significantly higher immunoreactivity in animals implanted with NM control probes compared to L1 probes for all time points, indicating a higher number of macrophages and activated microglia (Figures 7D-F). This significant difference was observed at each time point within the 100 m region (Table 2 and Figure 7C).

Iba1 is expressed in normal microglia and upregulated in activated microglia. Iba1 intensity plots showed similar trends as the ED-1 reactivity (Figures 8D-F). However, the Iba1 staining had a more diffuse microglia response zone (Figures 8A,B). Pairwise comparisons revealed no significant change between L1 and NM probe at week 1 (Table 2) although significance was seen at 4 and 8 weeks in the 0-100 μm area around the probes (Figure 8C).

3.4. Additional results

Quantitative analyses were performed for different depths along the probes' shaft at all time points. Differences were found between some depths and time points; however, no significant trends were observed to report here.

Several probes were retrieved after each time point and stained for β-tubulin III, a neuron specific marker. The L1 modified probes at the 4-week time point showed a significant attachment of neuronal processes (Figure 9A) while the NM probes did not shown any β-tubulin III positive staining (Figure 9B). Although the success rate of retrieving probes was

too low to perform any quantitative comparison, the fact that neurons and neuronal processes are directly attached to the L1 probe's surface is a significant finding.

4. Discussion

Silicon- based neural probes are used as tools to study the nervous system and as therapeutic strategies to restore lost function in the nervous system due to trauma or disease. Chronic implantation of these devices involves inevitable acute injury and chronic inflammation indicated by the loss of neurons and glial scaring [1, 14, 18, 44]. Current approaches to mitigate these responses include surface modification to promote neuronal attachment and/or delivery of anti-inflammatory, neuroprotective, and neurotrophic factors directly at the implant-tissue interface [25-27, 31, 32, 45, 46]. Although such strategies have shown to reduce the host brain response around the implant site to various degrees, significant improvement in *both* neuronal density and gliosis at the acute and chronic time points have not been demonstrated.

In this study, we demonstrate that the immobilization of neuron specific L1 protein on the surface of probes remarkably reduces gliosis response while promoting neuronal density at the implant tissue interface at both acute (1 week) and chronic (4 and 8 weeks) time points.

We studied the brain tissue response of 4 shank chronic Michigan probes, which produce multiple penetrating injuries and are known to lead to pronounced neuronal loss and glial activation [13, 47]. Staining for neuronal cell bodies showed a significant reduction of NeuN immunoreactivity around the non-modified (NM) control probes at all time points. The significant reduction of NeuN+ cells compared to background tissue was restricted to a 150 μm area around the probe-tissue interface indicating that neuronal loss is a localized interfacial event. In previous studies, Biran *et al.* has reported neuronal cell loss up to 120 μm from the single shank Michigan probes at 2 and 4-week time points [13]. McConnell *et al.* using four-shank Michigan probes also showed significant neuronal reduction compared to background verified by the NeuN marker up to 100 μm from the interface at 2 and 8 weeks. Uniquely in this study, a 16-week chronic time point of was examined to show an increased neuronal loss extending 300 μm away from the probe's interface, suggesting progressive neuronal degeneration [20].

We also observed a significant decrease of axonal density at the vicinity of the implant indicated by NF-200 staining, compared to background tissue at all time points. Biran *et al.* also reported this phenomenon at the 2 and 4 weeks end points [13]. McConnell *et al.* did not observe any significant difference in the NF-200 axonal marker for all time points, speculating that axons were spared or that this phenomenon was an indication of axonal sprouting [20]. One thing to note here is that the McConnell study used untethered probes, while the current study and Biran *et al.*'s study use tethered probes in order to better mimic functional probe applications. Using tethered implants have demonstrated to cause increased tissue reaction [18].

The neuronal response of the L1 modified probes was noticeably different from the NM control implants. The number of NeuN+ cells surrounding L1 modified probes did not decrease when compared to the background tissue from 1 to 8 weeks following implantation. Remarkably, we also found that the presence of L1 on the surface of the probe significantly increased axonal outgrowth towards the probe when compared to the NF background tissue staining. This significant increase in axonal density adjacent to the L1 implants was found at all time points. In addition, as observed after implant extraction, neurons and neurites were attached on the surface of the probes. This evidence suggests that the L1 on the surface of the probes interacted with the L1 on the axons of the nearby host

neurons, leading to enhanced neuronal adhesion and neurite outgrowth on and around the probes presumably via homophilic bindings. Throughout development, neurons are known to extend their axons via L1-L1 homophilic interactions [34, 48]. In addition to axonal extension, L1 has also shown to be a survival factor for neurons *in vitro* and *in vivo* [49]. Cerebellar neurons respond with a marked increase in cAMP levels [50], which is known to be effective in improving the survival of dopaminergic neurons and protecting them from the cytotoxic effects. The same mechanism could help the neurons that are injured/affected by the device insertion to survive the inflammatory and cytotoxic signals that lead to neuronal death. L1 has also been considered to be a potent molecule for neural regeneration. Zhang *et al.* has shown that GAP-43 and L1 co-expressed in Purkinje cells can act synergistically to switch these regeneration-incompetent CNS neurons into regeneration-competent phenotypes *in vivo* [51]. Here, we hypothesize that the high concentration of L1 on the surface of probes may also play a crucial role in promoting the regeneration of injured neurons present in close proximity of the probe insult.

For the glial responses, we observed similar trends around the NM probes at all time points as it has been previously reported in several studies [14, 17, 20, 25, 28, 31, 44]. During these previous studies, the microglia/macrophage cells were found adjacent to the NM implants indicating their early recruitment and activation. On the other hand, the astrocytic response became denser with time forming a tight sheath/scar tissue around the device. Here, we show the spatial distribution of reactive astrocytes surrounding the implants as determined by GFAP staining. GFAP immunoreactivity for both NM and L1 probe conditions increased as a function of time within the 100 μm region. It appears that reactive astrocytes progressively push neurons away from the recording zone, one of the suggested failure mechanism modes during single unit recordings [14, 17]. The L1 modified implant showed similar trends to the NM implant, although with a significant decrease of 78%, 83%, and 57% (week 1, 4, and 8 respectively) at the immediate intensity profile (0-20 μm) of the probe's interface. Vimentin is expressed in reactive astrocytes and meningeal cells. Meningeal cells are similar to fibroblasts but are found in the meninges. Meningeal fibroblasts stain for Vimentin but do not stain for GFAP and are known to migrate down the probe's shanks from the surface of the brain (pia and dura mater) to form the early basis for gliosis [22]. Vimentin in this study seemed to be more confined to the implant interface than the GFAP immunoreactivity, indicating the presence of fibroblasts closer to the implant interface due to the initial vascular injury. Compared to the NM probes, L1 implants indicated a significant decrease of Vimentin activity at all time points. This response to L1 probes agrees with a previous study that has shown L1 to be inhibitory to fibroblast attachment *in vitro* [35].

In addition, we stained for microglia cells using ED-1 and Iba1. ED-1+ cells, a combination of hematogenous macrophages and activated microglia, were much more prevalent adjacent to all implants observed at all time points. The presence of ED-1+ cells at the later time points indicates that local bleeding does not only occur during the acute injury. The initial implant vascular damage might increase the sustained activation of microglia next to the electrodes. It has also been suggested that ED-1 immune reaction is caused by or exacerbated by an increase in device motion due to electrode anchorage to the skull [18]. Remarkably, L1 modified implanted animals showed a significant reduction of ED-1 immunoreactivity at the electrode-tissue interface. Iba1 immunoreactivity showed similar trends to both tested implants, with a broader spatial distribution since Iba1 stains for all microglia present in the brain tissue.

The mechanisms for the reduction of microglia and astrocyte activation around the L1 modified probes are not known. We hypothesize the following mechanisms: 1) The surface bound L1 might specifically attract the nearby neurites onto the probe's surface and might

keep these neurons around the proximity of the probe while also keeping non-neuronal cells away from the implant, 2) Microglia and astrocytes are recruited and activated upon the presence of a trauma/foreign body. The L1 surface presents a biological surface that might disguise these cells in behaving less responsive to the foreign implant material, and 3) Microglia/macrophages are usually the cells that first respond to a foreign implant and they are often found to be most adjacent to the implant [14, 44]. These cells can have dramatically different functions from proinflammatory and degenerative, to anti-inflammatory and neuroprotective [19, 21]. The interaction of L1 on microglia and macrophage has not been studied. We speculate that L1 might have interacted with these cells, via unknown mechanisms, to turn on the anti-inflammatory pathways which lead to minimized gliosis and promote neuronal health and regeneration.

In summary, we report the cellular responses associated with the presence of the biomolecule L1 on the surface of silicon-based microelectrode arrays. Around all L1 modified probes, at all tested time points, we observed a decreased microglia and astrocyte reaction compared to the NM control probes. Most importantly, we saw a normal arrangement of neuronal bodies around the implant with a substantial increase of mature axons around and also attached onto the surface of the L1 modified probes. The chemical stability of this covalently bound protein layer *in vivo* is difficult to characterize. However, the long lasting biological effect observed up to 8 weeks suggests that 1) the L1 coating is stable for 8 weeks, or 2) perhaps more likely, it mitigated the initial inflammatory tissue response and provided a healthy substrate for neurons which later lay down their own growth matrix. Neuronal and dendritic loss at 16 weeks have been reported [20]. It would be appealing to run longer-term studies in the future, in order to further investigate whether this later stage of neuronal degeneration can be reduced or avoided using the L1 coating.

The surface immobilization of L1 presented here showed promising effect in improving neuronal density and mitigating gliosis around neural probes. The long lasting effect on neuronal density around the probe has not been previously demonstrated by other surface modification or drug delivery approaches. Although extensive detailed studies at the cellular and the molecular level are required to shed more light on the precise mechanisms responsible for this effect, the high neuronal density around the probe is expected to lead to better neural recording. Future studies involving longer time points and functional probes are essential in understanding the impact of the L1 induced biological effect on chronic neural recordings. Failure of chronic recordings may be caused by multiple factors and a single surface modification approach is not likely to solve the problem completely. The ultimate solution should be a combination of approaches that serve to mediate the mechanical, chemical, and biological differences between the micro-device and the neural tissue.

5. Conclusions

The present study demonstrates that covalent attachment of the neural adhesion protein L1 on silicon based electrode arrays significantly reduced the microglia and the astrocyte reaction, while maintaining the neuronal density and promoting axonal regeneration in close proximity to the probe-tissue interface. These results suggest that the L1 coating can be a promising strategy to improve biocompatibility of all types of neural probes in the brain and furthermore enhance their chronic recording performance.

Acknowledgments

The authors acknowledge Dr. Simon Watkins for imaging advice and confocal training at the Center for Biological Imaging of the University of Pittsburgh. The authors also thank Erika Rost and Giovanna Distefano for their technical assistance on histology. Funding for this research was supported in part by the National Institute of Health

R01NS062019, the Department of Defense TATRC grant WB1XWH-07-1-0716, and the National Science Foundation Grants 0748001, 0729869

References

1. Schwartz AB. Cortical neural prosthetics. Annu Rev Neurosci. 2004; 27:487–507. [PubMed: 15217341]
2. Kennedy PR, Bakay RA. Restoration of neural output from a paralyzed patient by a direct brain connection. Neuroreport. 1998; 9(8):1707–11. [PubMed: 9665587]
3. Hochberg LR, Serruya MD, Friehs GM, Mukand JA, Saleh M, Caplan AH, et al. Neuronal ensemble control of prosthetic devices by a human with tetraplegia. Nature. 2006; 442(7099):164–71. [PubMed: 16838014]
4. Donoghue JP, Nurmikko A, Black M, Hochberg LR. Assistive technology and robotic control using motor cortex ensemble-based neural interface systems in humans with tetraplegia. J Physiol. 2007; 579(Pt 3):603–11. [PubMed: 17272345]
5. Donoghue JP, Nurmikko A, Friehs G, Black M. Development of neuromotor prostheses for humans. Suppl Clin Neurophysiol. 2004; 57:592–606. [PubMed: 16106661]
6. Truccolo W, Friehs GM, Donoghue JP, Hochberg LR. Primary motor cortex tuning to intended movement kinematics in humans with tetraplegia. J Neurosci. 2008; 28(5):1163–78. [PubMed: 18234894]
7. Truccolo W, Hochberg LR, Donoghue JP. Collective dynamics in human and monkey sensorimotor cortex: predicting single neuron spikes. Nat Neurosci. 2010; 13(1):105–11. [PubMed: 19966837]
8. Donoghue JP. Connecting cortex to machines: recent advances in brain interfaces. Nat Neurosci. 2002; 5(Suppl):1085–8. [PubMed: 12403992]
9. Donoghue JP. Bridging the brain to the world: a perspective on neural interface systems. Neuron. 2008; 60(3):511–21. [PubMed: 18995827]
10. Friehs GM, Zerris VA, Ojakangas CL, Fellows MR, Donoghue JP. Brain-machine and brain-computer interfaces. Stroke. 2004; 35(11 Suppl 1):2702–5. [PubMed: 15486335]
11. Hatsopoulos NG, Donoghue JP. The science of neural interface systems. Annu Rev Neurosci. 2009; 32:249–66. [PubMed: 19400719]
12. Kubler A, Mushahwar VK, Hochberg LR, Donoghue JP. BCI Meeting 2005--workshop on clinical issues and applications. IEEE Trans Neural Syst Rehabil Eng. 2006; 14(2):131–4. [PubMed: 16792277]
13. Biran R, Martin DC, Tresco PA. Neuronal cell loss accompanies the brain tissue response to chronically implanted silicon microelectrode arrays. Exp Neurol. 2005; 195(1):115–26. [PubMed: 16045910]
14. Polikov VS, Tresco PA, Reichert WM. Response of brain tissue to chronically implanted neural electrodes. J Neurosci Methods. 2005; 148(1):1–18. [PubMed: 16198003]
15. Schwartz AB, Cui XT, Weber DJ, Moran DW. Brain-controlled interfaces: movement restoration with neural prosthetics. Neuron. 2006; 52(1):205–20. [PubMed: 17015237]
16. Vetter RJ, Williams JC, Hetke JF, Nunamaker EA, Kipke DR. Chronic neural recording using silicon-substrate microelectrode arrays implanted in cerebral cortex. IEEE Trans Biomed Eng. 2004; 51(6):896–904. [PubMed: 15188856]
17. Szarowski DH, Andersen MD, Retterer S, Spence AJ, Isaacson M, Craighead HG, et al. Brain responses to micro-machined silicon devices. Brain Res. 2003; 983(1-2):23–35. [PubMed: 12914963]
18. Kim YT, Hitchcock RW, Bridge MJ, Tresco PA. Chronic response of adult rat brain tissue to implants anchored to the skull. Biomaterials. 2004; 25(12):2229–37. [PubMed: 14741588]
19. Barron KD. Microglia: history, cytology, and reactions. J Neurol Sci. 2003; 207(1-2):98. [PubMed: 12614938]
20. McConnell GC, Rees HD, Levey AI, Gutekunst CA, Gross RE, Bellamkonda RV. Implanted neural electrodes cause chronic, local inflammation that is correlated with local neurodegeneration. J Neural Eng. 2009; 6(5):56003.

21. Schwartz M. Macrophages and microglia in central nervous system injury: are they helpful or harmful? J Cereb Blood Flow Metab. 2003; 23(4):385–94. [PubMed: 12679714]
22. Cui X, Wiler J, Dzaman M, Altschuler RA, Martin DC. In vivo studies of polypyrrole/peptide coated neural probes. Biomaterials. 2003; 24(5):777–87. [PubMed: 12485796]
23. Cui XY, Martin DC. Electrochemical deposition and characterization of poly(3,4-ethylenedioxythiophene) on neural microelectrode arrays. Sensors and Actuators B-Chemical. 2003; 89(1-2):92–102.
24. Ludwig KA, Uram JD, Yang J, Martin DC, Kipke DR. Chronic neural recordings using silicon microelectrode arrays electrochemically deposited with a poly(3,4-ethylenedioxythiophene) (PEDOT) film. J Neural Eng. 2006; 3(1):59–70. [PubMed: 16510943]
25. He W, McConnell GC, Bellamkonda RV. Nanoscale laminin coating modulates cortical scarring response around implanted silicon microelectrode arrays. J Neural Eng. 2006; 3(4):316–26. [PubMed: 17124336]
26. Zhong Y, Bellamkonda RV. Controlled release of anti-inflammatory agent alpha-MSH from neural implants. J Control Release. 2005; 106(3):309–18. [PubMed: 15978692]
27. Kim DH, Martin DC. Sustained release of dexamethasone from hydrophilic matrices using PLGA nanoparticles for neural drug delivery. Biomaterials. 2006; 27(15):3031–7. [PubMed: 16443270]
28. Spataro L, Dilgen J, Retterer S, Spence AJ, Isaacson M, Turner JN, et al. Dexamethasone treatment reduces astroglia responses to inserted neuroprosthetic devices in rat neocortex. Exp Neurol. 2005; 194(2):289–300. [PubMed: 16022859]
29. Shain W, Spataro L, Dilgen J, Haverstick K, Retterer S, Isaacson M, et al. Controlling cellular reactive responses around neural prosthetic devices using peripheral and local intervention strategies. IEEE Trans Neural Syst Rehabil Eng. 2003; 11(2):186–8. [PubMed: 12899270]
30. Wadhwa R, Lagenaur CF, Cui XT. Electrochemically controlled release of dexamethasone from conducting polymer polypyrrole coated electrode. J Control Release. 2006; 110(3):531–41. [PubMed: 16360955]
31. Zhong Y, Bellamkonda RV. Dexamethasone-coated neural probes elicit attenuated inflammatory response and neuronal loss compared to uncoated neural probes. Brain Res. 2007; 1148:15–27. [PubMed: 17376408]
32. Purcell EK, Thompson DE, Ludwig KA, Kipke DR. Flavopiridol reduces the impedance of neural prostheses in vivo without affecting recording quality. J Neurosci Methods. 2009; 183(2):149–57. [PubMed: 19560490]
33. Dihne M, Bernreuther C, Sibbe M, Paulus W, Schachner M. A new role for the cell adhesion molecule L1 in neural precursor cell proliferation, differentiation, and transmitter-specific subtype generation. J Neurosci. 2003; 23(16):6638–50. [PubMed: 12878705]
34. Rathjen FG, Schachner M. Immunocytological and biochemical characterization of a new neuronal cell surface component (L1 antigen) which is involved in cell adhesion. Embo J. 1984; 3(1):1–10. [PubMed: 6368220]
35. Webb K, Budko E, Neuberger TJ, Chen S, Schachner M, Tresco PA. Substrate-bound human recombinant L1 selectively promotes neuronal attachment and outgrowth in the presence of astrocytes and fibroblasts. Biomaterials. 2001; 22(10):1017–28. [PubMed: 11352083]
36. Guseva D, Angelov DN, Irintchev A, Schachner M. Ablation of adhesion molecule L1 in mice favours Schwann cell proliferation and functional recovery after peripheral nerve injury. Brain. 2009; 132(8):2180–95. [PubMed: 19541848]
37. Becker CG, Lieberoth BC, Morellini F, Feldner J, Becker T, Schachner M. L1.1 is involved in spinal cord regeneration in adult zebrafish. J Neurosci. 2004; 24(36):7837–42. [PubMed: 15356195]
38. Chen J, Wu J, Apostolova I, Skup M, Irintchev A, Kugler S, et al. Adeno-associated virus-mediated L1 expression promotes functional recovery after spinal cord injury. Brain. 2007; 130(4): 954–69. [PubMed: 17438016]
39. Chen J, Bernreuther C, Dihne M, Schachner M. Cell adhesion molecule l1-transfected embryonic stem cells with enhanced survival support regrowth of corticospinal tract axons in mice after spinal cord injury. J Neurotrauma. 2005; 22(8):896–906. [PubMed: 16083356]

40. Roonprapunt C, Huang W, Grill R, Friedlander D, Grumet M, Chen S, et al. Soluble cell adhesion molecule L1-Fc promotes locomotor recovery in rats after spinal cord injury. J Neurotrauma. 2003; 20(9):871–82. [PubMed: 14577865]
41. Azemi E, Stauffer WR, Gostock MS, Lagenaur CF, Cui XT. Surface immobilization of neural adhesion molecule L1 for improving the biocompatibility of chronic neural probes: In vitro characterization. Acta Biomater. 2008; 4(5):1208–17. [PubMed: 18420473]
42. Drake KL, Wise KD, Farraye J, Anderson DJ, BeMent SL. Performance of planar multisite microprobes in recording extracellular single-unit intracortical activity. IEEE Trans Biomed Eng. 1988; 35(9):719–32. [PubMed: 3169824]
43. Bhatia SK, Shriver-Lake LC, Prior KJ, Georger JH, Calvert JM, Bredehorst R, et al. Use of thiol-terminal silanes and heterobifunctional crosslinkers for immobilization of antibodies on silica surfaces. Anal Biochem. 1989; 178(2):408–13. [PubMed: 2546467]
44. Turner JN, Shain W, Szarowski DH, Andersen M, Martins S, Isaacson M, et al. Cerebral astrocyte response to micromachined silicon implants. Exp Neurol. 1999; 156(1):33–49. [PubMed: 10192775]
45. He W, Bellamkonda RV. Nanoscale neuro-integrative coatings for neural implants. Biomaterials. 2005; 26(16):2983–90. [PubMed: 15603793]
46. Kim DH, Wiler JA, Anderson DJ, Kipke DR, Martin DC. Conducting polymers on hydrogel-coated neural electrode provide sensitive neural recordings in auditory cortex. Acta Biomater. 2010; 6(1):57–62. [PubMed: 19651250]
47. Bjornsson CS, Oh SJ, Al-Kofahi YA, Lim YJ, Smith KL, Turner JN, et al. Effects of insertion conditions on tissue strain and vascular damage during neuroprosthetic device insertion. J Neural Eng. 2006; 3(3):196–207. [PubMed: 16921203]
48. Lagenaur C, Lemmon V. An L1-like molecule, the 8D9 antigen, is a potent substrate for neurite extension. Proc Natl Acad Sci USA. 1987; 84(21):7753–7. [PubMed: 3478724]
49. Hulley P, Schachner M, Lubbert H. L1 neural cell adhesion molecule is a survival factor for fetal dopaminergic neurons. J Neurosci Res. 1998; 53(2):129–34. [PubMed: 9671969]
50. Von Bohlen Und Halbach F, Taylor J, Schachner M. Cell type-specific effects of the neural adhesion molecules L1 and N-CAM on diverse second messenger systems. Eur J Neurosci. 1992; 4(10):896–909. [PubMed: 12106425]
51. Zhang Y, Bo X, Schoepfer R, Holtmaat AJ, Verhaagen J, Emson PC, et al. Growth-associated protein GAP-43 and L1 act synergistically to promote regenerative growth of Purkinje cell axons in vivo. Proc Natl Acad Sci USA. 2005; 102(41):14883–8. [PubMed: 16195382]

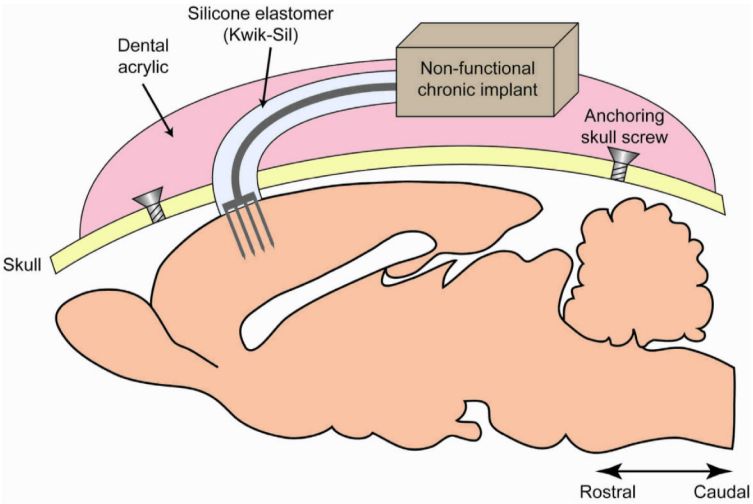

Figure 1.
Schematic representation of the non-functional (dummy) probe implantation in the rat cortex mimicking the same anchoring procedures as functional probes.

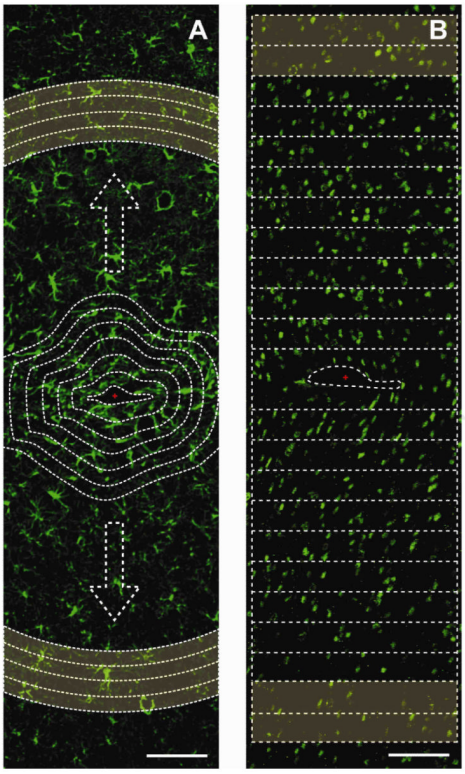

Figure 2.

Quantifications using ImageJ. (A) Example GFAP+ (green) stained image. The average gray scale intensity of pixels was quantified within 20 m bands from the initial probe interface (shown as the first dotted line) as a function of distance up to 520 μm away from the interface. Highlighted region is the background region chosen for each image (420-520 m bands) to normalize data. Scale bar 100 μm. (B) Example NeuN+ (green) stained image. NeuN+ cell counts using performed using watershed algorithms within 50 m increment boxes from each side of the probe's interface center (marked in red). Highlighted region is the background region used to normalize the NeuN+ cell counts (500-600 m). Scale bar 100 μm.

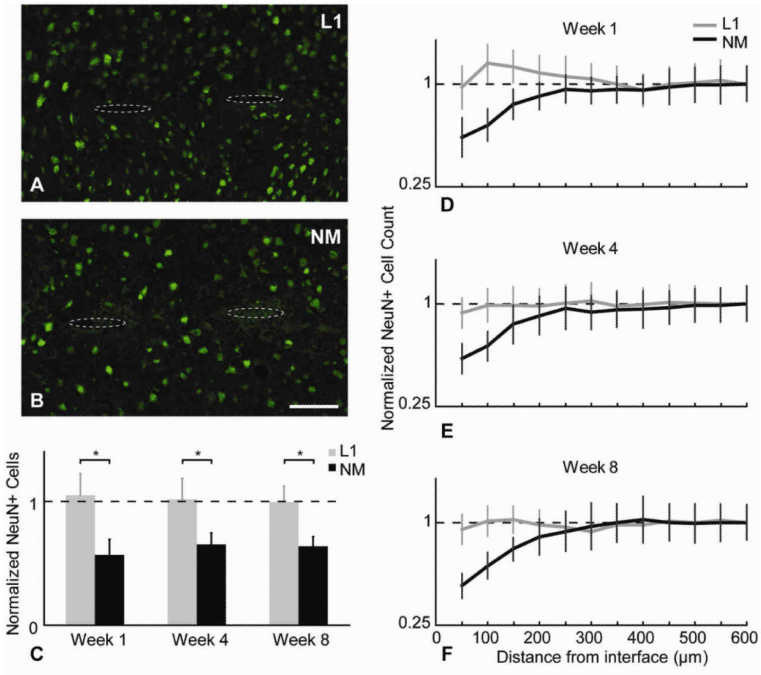

Figure 3.

NeuN analysis. (A,B) Representative images of NeuN+ (green) cells around the NM and L1 probes at week 8. Probe tracts shown with dotted ovals to assist visualization. Scale bar = 100 μm. (C) Normalized cell count differences between L1 and NM probes for the 0-100 μm region away from the interface at different time points (*$p<0.05$). (D-F) Normalized average NeuN+ cell number as a function of distance for all time points (mean ± s.e.m.).

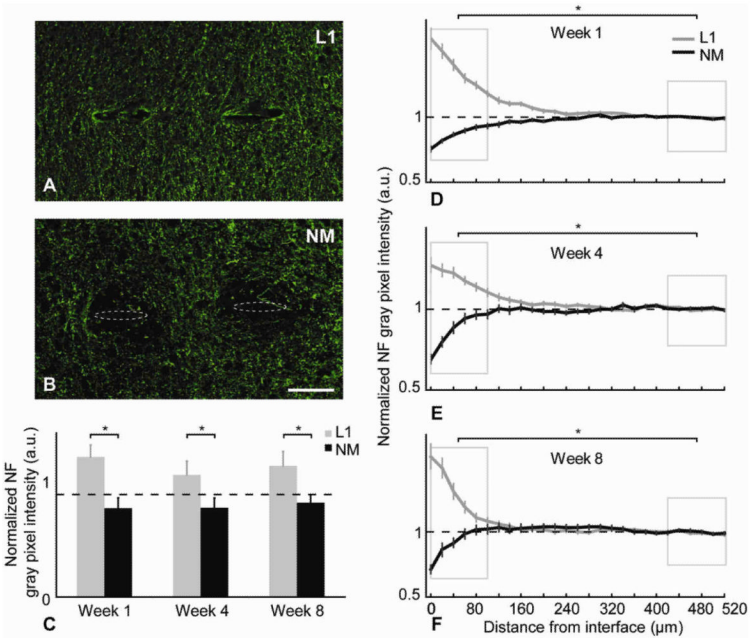

Figure 4.

NF analysis. (A,B) Representative images of NF+ (green) stained tissue at week 8. Probe tracts shown with dotted ovals to assist visualization. Scale bar = 100 μm. (C) Normalized NF intensity level differences between L1 and NM probes for the 0-100 μm region away from the interface at different time points (*p<0.05). (D-F) Normalized average NF intensity levels as a function of distance for all time points (mean ± s.e.m.). Boxed regions show statistical comparison of the intensity data between the 0-100 μm distances around the interface and the background for both L1 modified and NM probes was made (*p<0.05).

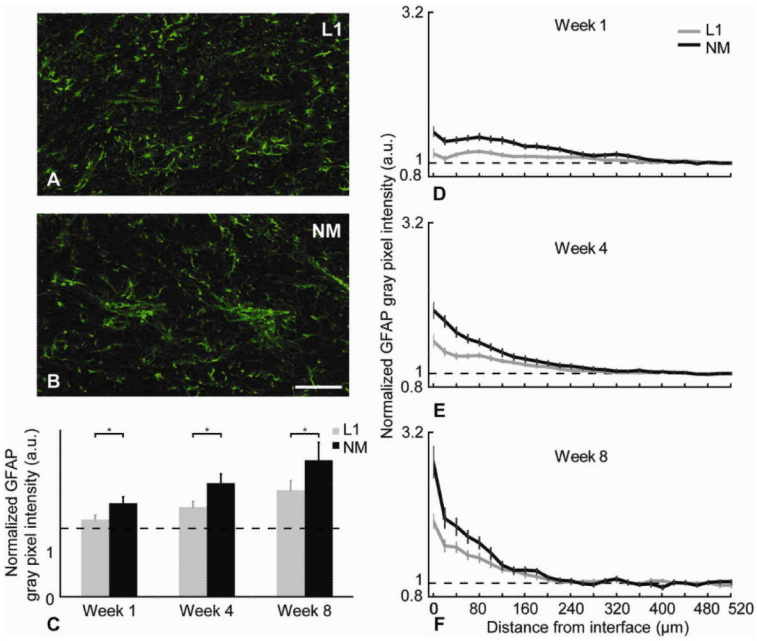

Figure 5.

GFAP analysis. (A,B) Representative images of GFAP+ (green) stained tissue at week 8. Scale bar = 100 μm. (C) Normalized GFAP intensity level differences between L1 and NM probes for the 0-100 μm region away from the interface at different time points (*$p<0.05$). (D-F) Normalized average GFAP intensity levels as a function of distance for all time points (mean ± s.e.m.).

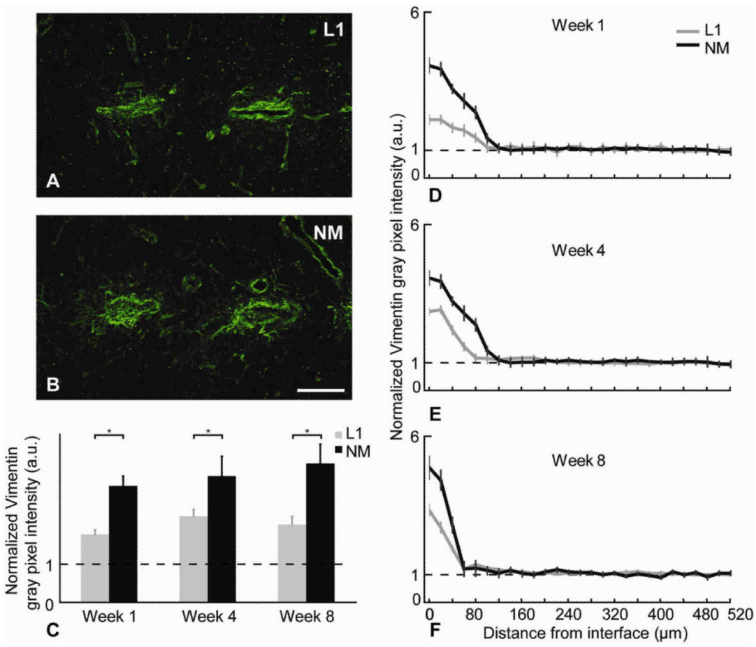

Figure 6.

Vimentin analysis. (A,B) Representative images of Vimentin+ (green) stained tissue at week 8. Scale bar = 100 μm. (C) Normalized Vimentin intensity level differences between L1 and NM probes for the 0-100 μm region away from the interface at different time points (*$p<0.05$). (D-F) Normalized average Vimentin intensity levels as a function of distance for all time points (mean ± s.e.m.).

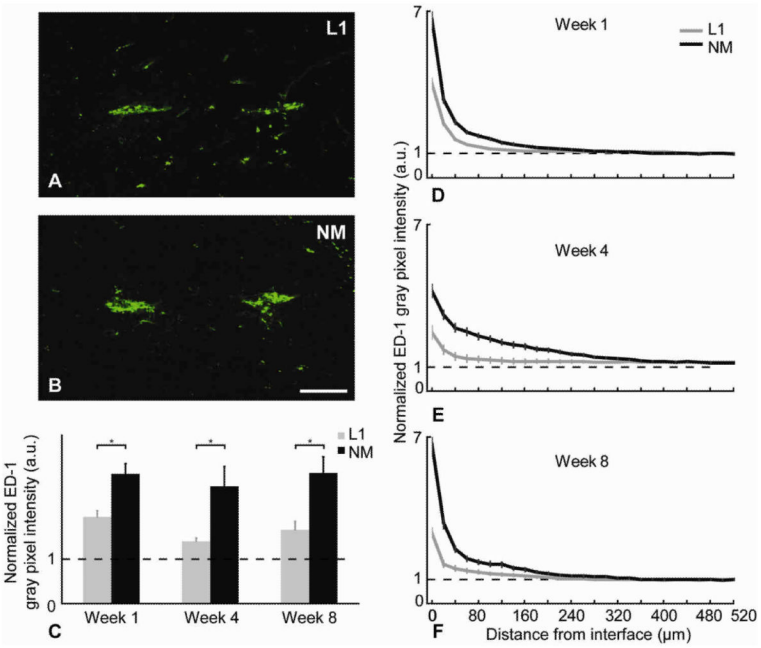

Figure 7.

ED-1 analysis. (A,B) Representative images of ED-1+ (green) stained tissue at week 8. Scale bar = 100 μm. (C) Normalized ED-1 intensity level differences between L1 and NM probes for the 0-100 μm region away from the interface at different time points (*$p<0.05$). (D-F) Normalized average ED-1 intensity levels as a function of distance for all time points (mean ± s.e.m.).

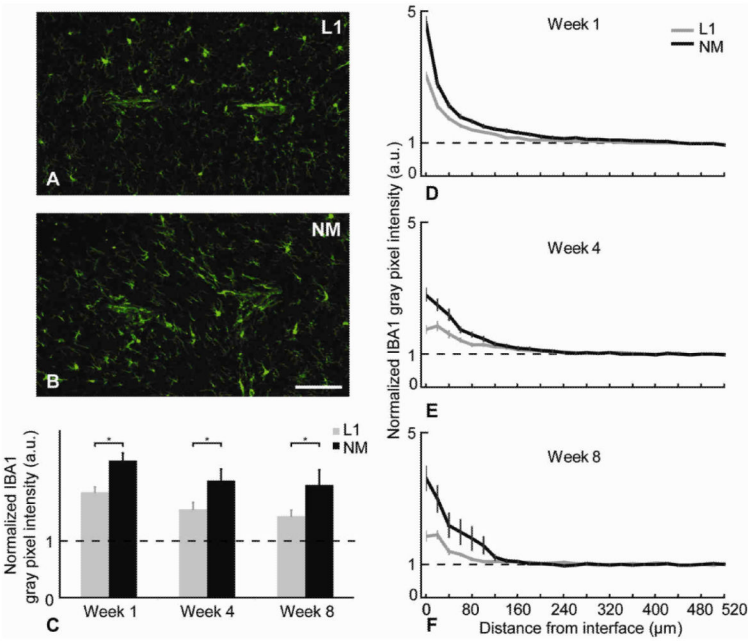

Figure 8.

Iba1 analysis. (A,B) Representative images of Iba1+ (green) stained tissue at week 8. Scale bar = 100 μm. (C) Normalized Iba1 intensity level differences between L1 and NM probes for the 0-100 μm region away from the interface at different time points (*p<0.05). (D-F) Normalized average Iba1 intensity levels as a function of distance for all time points (mean ± s.e.m.).

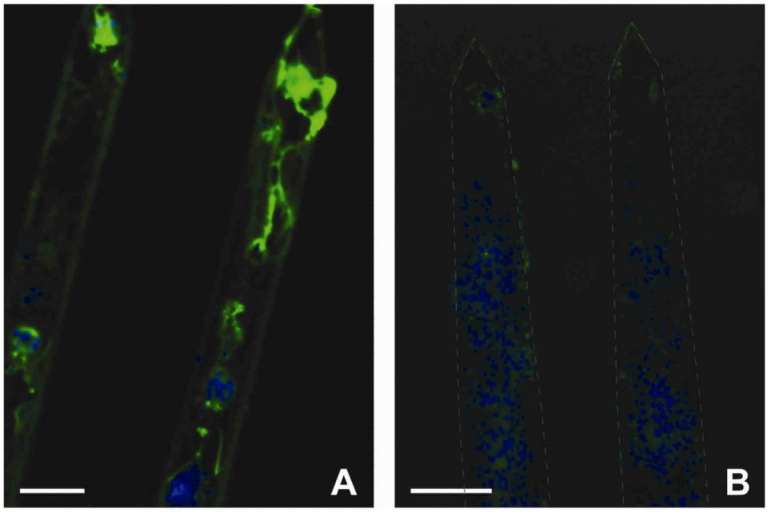

Figure 9.

Observation of neurons attached on the probes 4 weeks post-implantation. β-tubulin III (green) and Hoechst (blue). Scale bar = 100 μm. (A) L1 modified probe showed attachment of neurons even after fixation and probe removal. (B) NM probe showed no attachment of neurons but other cells were present on the probe as demonstrated by the Hoechst counterstain.

Table 1

Summary of antibodies

Antibodies	Host	Isotype	Clonality	Vendor	Dilution	Specificity
NeuN	mouse	IgG1	monoclonal	Millipore	1:500 (2 μg/ml)	Neuronal nuclei
NF200	mouse	IgG1	monoclonal	Millipore	1:500 (0.2 μg/ml)	Mature axons
β-tubulin III (Tuj-1)	mouse	IgG2b	monoclonal	Sigma	1:500 (2 μg/ml)	CNS and PNS neurons
GFAP	rabbit	IgG	polyclonal	Dako	1:500 (0.2 μg/ml)	Mature astrocytes
Vimentin	mouse	IgG1	monoclonal	Millipore	1:500 (2 μg/ml)	Immature and reactive astrocytes, microglia, endothelial cells, and fibroblasts
ED-1 (CD68)	mouse	IgG1	monoclonal	Serotec	1:500 (0.2 μg/ml)	Activated microglia/macrophages
Iba1	rabbit	IgG2b	monoclonal	AbCam	1:250 (1 μg/ml)	Microglia/macrophages

Biomaterials. Author manuscript; available in PMC 2012 July 11.

Table 2

Calculated p-values of 100 μm increment levels for each antibody comparing L1 modified versus the NM probe image analysis data (*p<0.05)

	Distance from interface	NeuN	NF	GFAP	Vimentin	ED-1	Iba1
week 1	0-100 μm	0.018*	0.013*	0.032*	0.014*	0.049*	0.052
	100-200 μm	0.047*	0.032*	0.062	0.090	0.092	0.090
	200-300 μm	0.084	0.278	0.121	0.853	0.156	0.123
	300-400 μm	0.125	0.302	0.256	0.367	0.244	0.233
	400-500 μm	0.151	0.432	0.551	0.688	0.322	0.421
week 4	0-100 μm	0.028*	0.042*	0.021*	0.029*	0.021*	0.042*
	100-200 μm	0.048*	0.095	0.077	0.140	0.055	0.080
	200-300 μm	0.086	0.177	0.176	0.455	0.089	0.223
	300-400 μm	0.122	0.353	0.104	0.148	0.232	0.320
	400-500 μm	0.115	0.359	0.284	0.508	0.200	0.523
week 8	0-100 μm	0.030*	0.030*	0.047*	0.092	0.001*	0.032*
	100-200 μm	0.046*	0.099	0.097	0.124	0.084	0.120
	200-300 μm	0.214	0.145	0.109	0.202	0.098	0.245
	300-400 μm	0.134	0.412	0.115	0.283	0.250	0.411
	400-500 μm	0.177	0.546	0.221	0.537	0.314	0.442

Biomaterials. Author manuscript; available in PMC 2012 July 11.